DOI: 10.1002/ejic.201100707

A Facile Approach for the Synthesis of Ag-Coated Fe_3O_4@TiO_2 Core/Shell Microspheres as Highly Efficient and Recyclable Photocatalysts

Yongxing Zhang,[a,b] Xinyao Yu,[b] Yong Jia,[b] Zhen Jin,[b] Jinhuai Liu,*[b] and Xingjiu Huang*[b]

Keywords: Nanoparticles / Silver / Iron / Titanium / Magnetic properties / Photocatalyst / Organic pollutants

A facile, green, and efficient approach for the fabrication of Ag-coated Fe_3O_4@TiO_2 microspheres with a good core/shell structure has been demonstrated. The protocol employed involves the coating of successive layers of TiO_2 nanoparticles on to a magnetic core using a vapor–thermal method at low temperature followed by the deposition of silver nanoparticles on the surface of the Fe_3O_4@TiO_2 microspheres through a photochemical route. The Ag-coated Fe_3O_4@TiO_2 microspheres show excellent magnetic properties at room temperature. The photocatalytic properties of the products were investigated for the degradation of organic dyes. The loading of Ag nanoparticles coated on to the surface of the Fe_3O_4@TiO_2 microspheres was controlled by changing the UV photoreduction time. The photocatalytic degradation rates were found to increase with the Ag nanoparticle loading until a maximum photodegradation rate was reached, further increasing the Ag loading led to a decrease in the photodegration rate. Furthermore, compared with that of Degussa P25 titania and uncoated Fe_3O_4@TiO_2 microspheres, the products have better photocatalytic activity. The renewable photocatalytic activity of the microspheres was also examined. The results indicate that the catalytic activity was still present after recycling the photocatalysts five times. Thus, the Ag-coated Fe_3O_4@TiO_2 core/shell microspheres can serve as effective and conveniently recyclable photocatalysts.

1. Introduction

Over the past few decades, photocatalytic degradation of organic pollutants in waste water using semiconductor nanomaterials has attracted much attention. Among various oxide semiconductor photocatalysts, titania (TiO_2)[1–3] has been proven to be the most suitable for widespread environmental applications because of its high chemical stability, lack of toxicity, and excellent degradation capacity for organic pollutants. However, on the basis of practicality, there are some major disadvantages for the application of such nanomaterials in treating waste water. For example, although monodispersed TiO_2 nanomaterials with high surface areas and excellent photocatalytic activity have been successfully prepared,[4–7] it is very inconvenient to recycle these materials because of their good dispersive properties. Conventional separation methods, including centrifugation and filtration, may lead to loss of the catalysts. In particular, centrifugation requires large amounts of energy, which may cause secondary pollution. On the other hand, photocatalysts fixed on the thin films have been successfully prepared,[7–12] which can allow easy recovery of photocatalysts. However, the activity of such photocatalysts is considerably reduced because the effective surface area of photocatalysts is significantly decreased.

In recent years, immobilizing catalysts on to the surface of magnetic nano- or microparticles has been an effective way of solving the problem described above, as they can be separated easily from the solution with the help of an external magnet. This approach may prevent the agglomeration of the catalyst particles during recovery and can increase the durability of the catalysts. There are two methods for immobilizing catalysts on to the surface of magnetic nano- or microparticles. One method is to directly immobilize the catalyst on to the surface of magnetic nano- or microparticles and the other is to indirectly immobilize the catalyst on to the surface of magnetic nano- or microparticles, which are modified with an intermediate barrier layer of silicon oxide (SiO_2). Wang et al.[13] have reported the synthesis of magnetic (γ-Fe_2O_3@SiO_2)$_n$@TiO_2 hybrid nanoparticles with fine particles of γ-Fe_2O_3@SiO_2 dispersed in the titania matrix. SiO_2 was used as a barrier layer in order to avoid interactions between the magnetic core and the TiO_2 coating after calcination.[14–18] However, the superparamag-

[a] Department of Chemistry, University of Science and Technology of China,
Hefei, Anhui 230026, P. R. China
[b] Research Center for Biomimetic Functional Materials and Sensing Devices, Institute of Intelligent Machines, Chinese Academy of Sciences,
Hefei, Anhui 230031, P. R. China
Fax: +86-551-5592420
E-mail: xingjiuhuang@iim.ac.cn
jhliu@iim.ac.cn

Supporting information for this article is available on the WWW under http://dx.doi.org/10.1002/ejic.201100707 or from the author.

netic characteristic of the hybrid nanoparticles significantly decreased after calcination. To minimize the heat treatment step, a modified sol–gel route was adopted to deposit crystalline TiO_2 directly on to the magnetic cores.[19] However, the photoactive TiO_2 layer did not form a uniform coating on the surface of the magnetic cores; rather, they formed patches on the surface. Lee et al.[20] have reported a magnetic photocatalyst prepared by controlled hydrolysis and condensation of titanium bisammonium lactato dihydroxide in the presence of polyethyleneimine, which focused on the synthesis of uniform photoactive crystalline (anatase) TiO_2 layers on the magnetic cores (barium ferrite) using a nonalkoxide TiO_2 precursor in water at low temperature (95 °C). Xuan et al.[21] have reported the fabrication of magnetically-separable photocatalysts with hollow nanostructures through a PSA template method at relatively low temperature (160 °C). However, both of the methods for the preparation of the magnetic photocatalyst were very complicated. Therefore, the synthesis of magnetic anatase TiO_2 nanoparticles with uniform size by a simple method without calcination has become a pressing need not only for fundamental interest but also for improved efficiency.

It is well known that the large band gap and low quantum yield of pure TiO_2 prevent its use in practical applications, although improvements have been made by increasing surface area and reducing defect sites.[22] Enhancement of the photocatalytic activity of TiO_2 is another important task for applications of heterogeneous photocatalysts in the future. Noble metals such as Ag, Au, Pt, and Pd deposited on TiO_2 surfaces enhance the photocatalytic activity of TiO_2. This is mainly due to the noble metals acting as electron traps, which promote interfacial charge transfer processes in the composites.[23] Thus, highly efficient photocatalysts that are modified with noble metals have been prepared in recent years.[24–28] However, it is difficult to recycle these photocatalysts.

The aim of this study is to obtain magnetically separable, recyclable, highly efficient photocatalysts, which are easy to synthesize without high-temperature treatment. We report the preparation of Fe_3O_4@TiO_2 microspheres, with a very good core/shell structure, using a simple vapor–thermal method at a relatively low temperature. Due to the low temperature of the experiment, the magnetic properties and photocatalytic activity of the samples do not deteriorate. Moreover, hydrolysis of the titanium precursor with water vapor is a newly developed method to synthesize nanosized anatase TiO_2. The anatase TiO_2 nanoparticles on the surface of the Fe_3O_4 microspheres exhibit high photocatalytic activity due to their large specific surface area and high crystallinity.[29] Ag nanoparticles, which are well deposited on the surface of the Fe_3O_4@TiO_2 microspheres by a photochemical route, combine with TiO_2 to form the Ag–TiO_2 heterostructure. The heterostructure can improve the separation of photogenerated electron-hole pairs, and thus enhance the photocatalytic activity of the Fe_3O_4@TiO_2 microspherical photocatalyst. At the same time, the renewable photocatalytic activity of the microspheres was also examined.

2. Results and Discussion

2.1 Characterization of Photocatalysts

Parts a–c of Figure 1 show scanning electron microscopy (SEM) images of the Fe_3O_4 microspheres, Fe_3O_4@TiO_2 microspheres, and Ag-coated Fe_3O_4@TiO_2 microspheres, respectively. It is clear that the sample is composed of many nearly monodispersed spherical particles with diameters of about 350 nm from Figure 1 (a). Furthermore, Figure 1 (a) also shows that the boundary of the Fe_3O_4 microspheres is very obvious. After the Fe_3O_4 microspheres were immersed in a mixed solution of ethanol and tetrabutyl titanate (TBOT) by the vapor-thermal method, the boundary of the microspheres became unclear; see Figure 1 (b). Moreover, the average particle diameter increased from 350 to 450 nm after the coating process, which indicates the precipitation of a ca. 100 nm thick TiO_2 shell on the Fe_3O_4 core. The effect of water vapor on promoting the hydrolysis of TBOT at different temperatures on the surface of the Fe_3O_4 microspheres was investigated. It was found that the TiO_2 shell on the surface of the Fe_3O_4 microspheres was difficult to form at 120 °C; however, at 150 or 180 °C, a uniform TiO_2 shell was formed on the surface of the Fe_3O_4 microspheres (Figure S1). We propose that there was not enough water vapor to promote the hydrolysis of TBOT at 120 °C, which resulted in the formation of a nonuniform shell on the surface of the Fe_3O_4 microspheres. The crystallite size of TiO_2 prepared at 180 °C was larger than that prepared at both 150 and 120 °C (see Supporting Information, Figure S1 c). In this research, the magnetic properties are considered to be affected by high temperature, so 150 °C was selected as the optimum temperature. In addition, the thickness of the TiO_2 shell on the surface of the Fe_3O_4 microspheres was easily tuned by modulating the amount of TBOT in the reaction medium (Figure S2). During the synthesis, the ethanol evaporates first as it has a lower boiling point than water, and the water vapor promotes the hydrolysis of TBOT. It is proposed that the surface of the Fe_3O_4 micro-

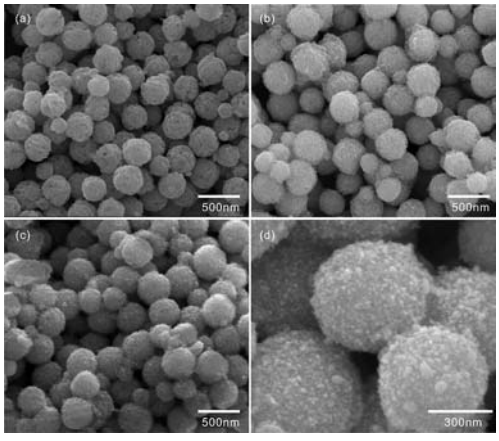

Figure 1. SEM images of (a) Fe_3O_4 microspheres, (b) Fe_3O_4@TiO_2 microspheres, and (c) Ag-coated Fe_3O_4@TiO_2 microspheres; (d) high-magnification SEM image of Ag-coated Fe_3O_4@TiO_2 microspheres.

spheres acts as nucleation sites during the initial stage of TiO_2 formation, and the as-formed TiO_2 nuclei subsequently act as nucleation sites for further deposition of TiO_2 nanoparticles, which leads to layer-by-layer assembly.

A SEM image of the Ag-coated Fe_3O_4@TiO_2 microspheres is shown in Figure 1 (c), from which it can be seen that Ag nanoparticles have adhered to the surface of the Fe_3O_4@TiO_2 microspheres. To get more information about the structure of the sample, it was further investigated by high-magnification SEM (Figure 1 d) which clearly shows many Ag nanoparticles on the surface of the Fe_3O_4@TiO_2 microspheres. Photodeposition of Ag nanoparticles on the surface of the Fe_3O_4@TiO_2 microspheres was carried out under UV irradiation in an aqueous $Ag(NH_3)_2^+$ solution. It is well known that the photochemical route is a promising way to form noble metal–semiconductor nanocomposites in situ by reducing the noble metal ions adsorbed on to the surface of a semiconductor.[30–31] An electron-hole pair is formed in the TiO_2 nanostructure under irradiation with UV light (Scheme 1).[32] In this process, the generated conduction band electrons can reduce $Ag(NH_3)_2^+$ absorbed on the TiO_2 surface, which leads to the direct deposition of silver nanoparticles on the surface of the Fe_3O_4@TiO_2 microspheres in the absence of organic linking molecules or other chemical reductants. The Ag nanoparticles produced by photoreduction can access any part of the surface of Fe_3O_4@TiO_2 microspheres that is illuminated by UV light. $AgNO_3$ aqueous solutions were used as reaction media under UV irradiation. However, well dispersed Ag nanoparticles on the surface of the Fe_3O_4@TiO_2 microspheres were not obtained (Figure S3). Compared with $AgNO_3$, $Ag(NH_3)_2^+$ can limit the concentration of free Ag ions in solution, thus, well dispersed Ag nanoparticles can be formed under UV irradiation.

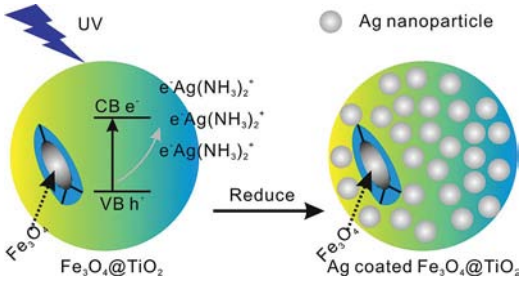

Scheme 1. Photochemical route for the formation of Ag-coated Fe_3O_4@TiO_2 microspheres. CB: conduction band; VB: valence band; e^-: photoexcited electrons; h^+: photoexcited holes.

The well coated Fe_3O_4@TiO_2 microspheres can also clearly be seen from TEM images (Figure 2 a). Figure 2 (b) shows that the thickness of the shell is about 100 nm, which agrees with the SEM results. Moreover, the image also shows that ultrafine Ag nanoparticles are well dispersed on the surface of the Fe_3O_4@TiO_2 microspheres. A high-resolution (HR)TEM image (Figure 2 c) reveals the formation of a Ag–TiO_2 heterostructure, in which metallic Ag nanoparticles and the TiO_2 layer join. The lattice fringe spacings of 0.241 and 0.357 nm observed from the Ag–TiO_2 HRTEM image correspond to the (111) plane of Ag and (101) plane of anatase TiO_2, respectively (JCPDS card No. 04-0783 and No. 21-1272).

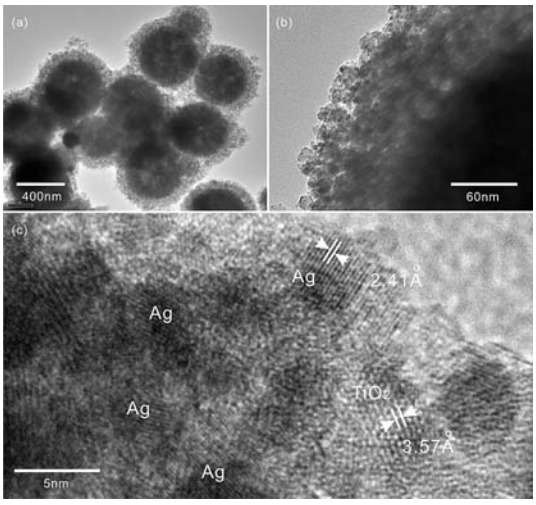

Figure 2. (a) and (b) TEM image of as-prepared Ag-coated Fe_3O_4-@TiO_2 microspheres, and (c) HRTEM image of Ag-coated Fe_3O_4-@TiO_2 microspheres.

In order to further confirm the presence of both TiO_2 and Ag nanoparticles on the surface of the Fe_3O_4 microspheres, samples were analyzed by electron mapping image analysis (Figure 3). The images were acquired by visualizing the inelastically scattered electrons in the energy loss windows for elemental O, Ti, Fe, and Ag. The different color areas shown in parts b–e of Figure 3 indicate O-, Ti-, Fe-, and Ag-enriched areas of the sample, respectively, which indicate the presence of both TiO_2 and Ag in the outer surface of the Fe_3O_4 microspheres. The images also show that the TiO_2 and Ag nanoparticles are well dispersed on the

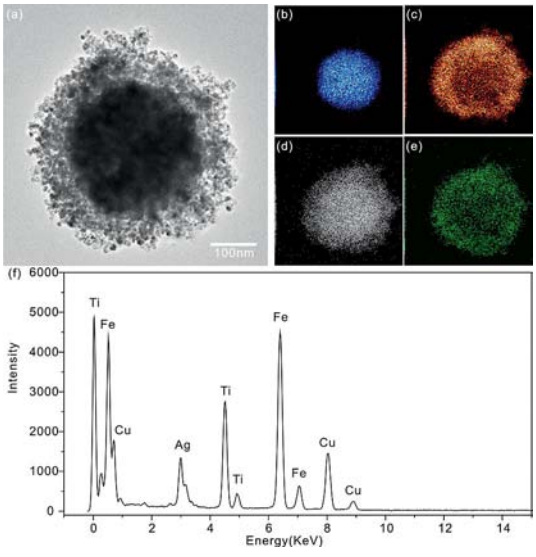

Figure 3. TEM images of (a) the Ag-coated Fe_3O_4@TiO_2 microspheres. Electron energy loss: (b) O, (c) Ti, (d) Fe, and (e) Ag element mapping images of the Ag-coated Fe_3O_4@TiO_2 microspheres. (f) EDS data of the Ag-coated Fe_3O_4@TiO_2 core/shell microspheres.

surface of the Fe_3O_4 microspheres. The energy dispersive spectroscopic (EDS) analysis (Figure 3 f) of the Ag-coated Fe_3O_4@TiO_2 microspheres reveals the existence of Ti, Fe, and Ag elements (copper signals are present from the copper grid support).

XRD was used to determine the phase structure of the samples. Figure 4 (a) shows a typical XRD pattern of the Fe_3O_4 microsphere samples, and all of the diffraction peaks can be readily indexed to the orthorhombic phase of Fe_3O_4 (JCPDS card No. 75-1609). The XRD pattern of the Fe_3O_4@TiO_2 microspheres (Figure 4 b) shows that, compared with Figure 4 (a), additional peaks appear, which can be attributed to the anatase phase of TiO_2 [JCPDS card No. 21-1272, space group: $I4_1/amd$ (1 4 1)] with a lattice constant a = 3.57 Å, marked A in Figure 4 (b). This suggests that the sample contains both anatase TiO_2 and orthorhombic Fe_3O_4 phases. The peaks of the anatase TiO_2 phase are from the TiO_2 shells and those of the orthorhombic Fe_3O_4 phase from Fe_3O_4 cores. This is consistent with our HRTEM observations. The typical XRD pattern of the Ag-coated Fe_3O_4@TiO_2 sample is shown in Figure 4 (c). In addition to the diffraction peaks that correspond to Fe_3O_4 and TiO_2, there are four other diffraction peaks (labeled S). These diffraction peaks were easily indexed to the cubic phase of Ag (JCPDS card No. 04-0783) with a lattice constant a = 2.41 Å, which is also consistent with our HRTEM observations. However, because of the low content of Ag, the intensity of the XRD pattern of Ag is weak.

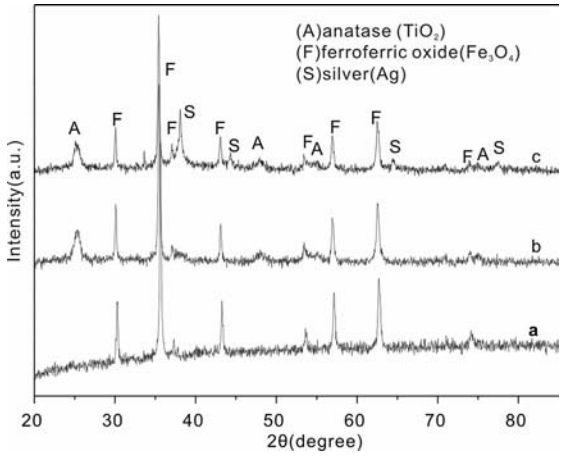

Figure 4. Wide-angle XRD patterns of (a) Fe_3O_4 microspheres, (b) Fe_3O_4@TiO_2 microspheres, and (c) Ag-coated Fe_3O_4@TiO_2 microspheres.

The texture of the as-prepared samples was characterized by N_2 physisorption experiments, and the corresponding N_2 adsorption–desorption isotherms and pore size distributions are shown in Figure 5. It can be seen that both the Ag-coated Fe_3O_4@TiO_2 microspheres and the Fe_3O_4@TiO_2 microspheres have type IV isotherms and type H3 hysteresis loops (according to IUPAC classification),[33] which suggests that they are mesoporous structures. The pores appear to be narrow slits, and the prepared particles are plate-like. However, the porous nature of the Fe_3O_4 microspheres can be neglected due to the small specific surface area and total pore volume. The hysteresis loops of the Ag-coated Fe_3O_4@TiO_2 microspheres and the Fe_3O_4@TiO_2 microspheres in the lower relative pressure range ($0.4 < P/P_0 < 0.9$) is related to finer intra-aggregated pores within the primary agglomerated particles (TiO_2 and Ag shell or TiO_2 shell) and that in the higher relative pressure range ($0.9 < P/P_0 < 1$) is associated with larger interaggregated pores between the secondary aggregated particles. This bimodal mesopore size distribution was confirmed by the corresponding pore size distributions (inset in Figure 5). The samples contain small intra-aggregated mesopores with a peak pore of ca. 12.4 nm and larger interaggregated mesopores (peak pore at 68.4 nm). The smaller mesopores reflect porosity within the TiO_2 and Ag shells or TiO_2 shells, whereas larger mesopores can be related to the pores formed between aggregated Ag-coated Fe_3O_4@TiO_2 microspheres or Fe_3O_4@TiO_2 microspheres. These mesoporous structures can be directly observed from the SEM and TEM images shown in Figures 1 and 2, respectively.

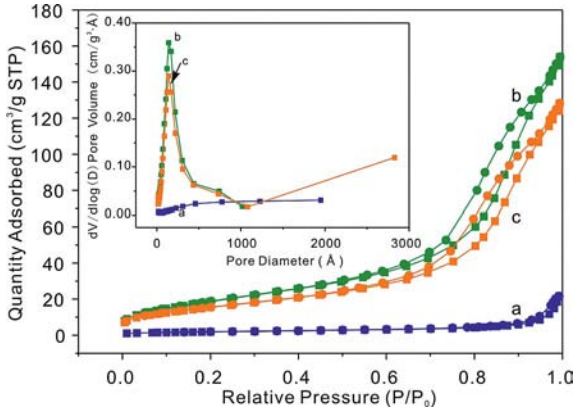

Figure 5. Nitrogen adsorption–desorption isotherms and the corresponding pore size distribution curves (inset) of the (a) Fe_3O_4 microspheres, (b) Fe_3O_4@TiO_2 microspheres, and c) Ag-coated Fe_3O_4@TiO_2 microspheres.

The quantitative texture information of the as-synthesized samples, such as Brunauer–Emmett–Teller (BET) surface areas and pore diameters, are summarized in Table 1. From the data, we can see that the Fe_3O_4@TiO_2 microspheres possess a large BET surface area and a high pore volume. The BET surface area and pore volume of the Ag-coated Fe_3O_4@TiO_2 microspheres is slightly smaller after the deposition of the Ag nanoparticles. The Fe_3O_4 microspheres have the smallest BET surface area and pore volume.

Table 1. Physical properties of the different samples.

Sample	BET [$m^2 g^{-1}$]	Pore diameter [nm]	Pore volume [$cm^3 g^{-1}$]
Fe_3O_4 microspheres	7.0	19.3	0.03
Fe_3O_4@TiO_2 microspheres	71.0	12.2	0.22
Ag-coated Fe_3O_4@TiO_2 microspheres	57.5	12.4	0.18

The magnetic hysteresis loops of the as-obtained Fe_3O_4 microspheres, Fe_3O_4@TiO_2 microspheres, and Ag-coated Fe_3O_4@TiO_2 microspheres are displayed in Figure 6 (a). All of the samples show ferromagnetic behavior at room temperature. The magnetic saturation (*Ms*) values of the Fe_3O_4 microspheres, Fe_3O_4@TiO_2 microspheres, and Ag-coated Fe_3O_4@TiO_2 microspheres are 77.5, 38.7, and 36.8 emu g^{-1}, respectively. It is worth noting that the *Ms* value of the Fe_3O_4 microspheres is significantly higher than that of the Fe_3O_4@TiO_2 microspheres and Ag-coated Fe_3O_4@TiO_2 microspheres, which is because the Fe_3O_4 microspheres are coated with a layer of anatase TiO_2 in the Fe_3O_4@TiO_2 microspheres and Ag-coated Fe_3O_4@TiO_2 microspheres. The small decrease in the *Ms* value of the Ag-coated Fe_3O_4-@TiO_2 microspheres compared to that of the Fe_3O_4@TiO_2 microspheres can be attributed to the slight increase of mass and size due to the adherence of Ag nanoparticles on to the surface of the magnetic composites. Furthermore, it can be seen that that there are no significant changes in the coercivity from the enlarged view of the central loop of the samples (Figure 6 b). Such excellent magnetic properties imply strong magnetic responsivity on the microspheres, which enables them to be recycled easily from solution with the help of an external magnetic force. Figure 6 (c) shows three photographs of a vessel containing the aqueous Ag-coated Fe_3O_4@TiO_2 microspheres. Figure 6 (c1) shows that the Ag-coated Fe_3O_4@TiO_2 microspheres are well dispersed in the aqueous solution. Figure 6 (c2) shows that complete magnetic separation of the Ag-coated Fe_3O_4@TiO_2 microspheres was achieved in 2 min by placing a magnet near the vessel. Then, the vessel was shaken several seconds after the magnet was removed, and the Ag-coated Fe_3O_4@TiO_2 microspheres were redispersed in the aqueous solution (Figure 6 c3). These photographs further demonstrate that easy, fast separation and redispersion of the Ag-coated Fe_3O_4@-TiO_2 microspheres can be realized.

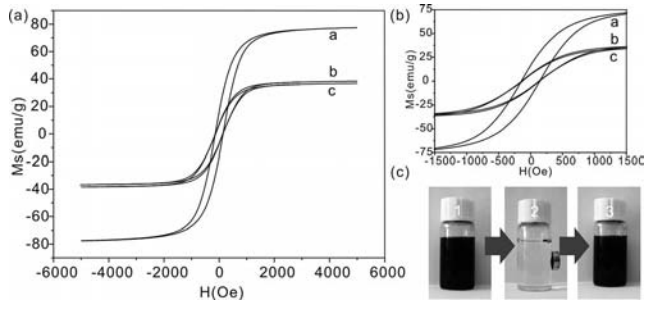

Figure 6. (a) Magnetic hysteresis loops and (b) the enlarged view of the central loops of a) Fe_3O_4 microspheres, b) Fe_3O_4@TiO_2 microspheres, and c) Ag-coated Fe_3O_4@TiO_2 microspheres, (c) photographs of 1) a 1×10^{-5} M methylene blue (MB) solution after UV irradiation for ca. 35 min with dispersed Ag-coated Fe_3O_4@TiO_2 microspheres, 2) the solution after magnetic separation using an external magnetic field, and 3) the 1×10^{-5} M MB aqueous solution with redispersed Ag-coated Fe_3O_4@TiO_2 microspheres after shaking.

2.2 Photocatalytic Activity

2.2.1 Effect of Ag Loading on the Photocatalytic Activity of Ag-Coated Fe_3O_4@TiO_2 Microspheres

Enhanced photocatalytic activity of the Fe_3O_4@TiO_2 microspheres was achieved by combining the Fe_3O_4@TiO_2 microspheres with Ag nanoparticles, which produced a "charge separation effect", which increases the lifetime of the photogenerated excitons.[34,35] When Ag nanoparticles are in contact with the Fe_3O_4@TiO_2 microspheres, they act as electron scavengers and can effectively suppress the electron-hole recombination. However, Ag nanoparticles deposited on to the surface of the Fe_3O_4@TiO_2 microspheres can decrease the active catalytic sites on the surface, thus there is a delicate balance between the charge-separation enhancement and the decrease in the active surface area.[34–35] In this study, we controlled the loading of the Ag nanoparticles coated on the surface of the Fe_3O_4@TiO_2 microspheres by changing the UV photoreduction time. Figure 7 shows the effect of different loadings of Ag nanoparticles on the photocatalytic activity of the Fe_3O_4@TiO_2 microspheres. As shown in Figure 7 (a), the Fe_3O_4@TiO_2 microspheres [sample a (0 mol-% Ag)] display the lowest photocatalytic activity. As the loading of Ag nanoparticles increases, the photocatalytic activity of the samples [samples b (1.00 mol-% Ag) and c (1.52 mol-% Ag)] increases. When the UV photoreduction time was 5 h (sample c), the photocatalytic activity reaches a maximum. When the loading was further increased, the photocatalytic activity [sam-

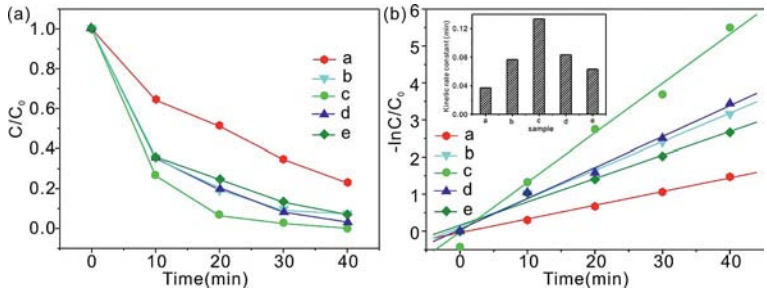

Figure 7. (a) The kinetic curve of the photodegradation of MB. (b) Comparison of first-order degradation rates of MB; Inset: reaction rate constants for MB degradation. The loading of the Ag nanoparticles was controlled by varying the UV photoreduction time t = 0 h [sample a (0 mol-% Ag)], 3 h [sample b (1.00 mol-% Ag)], 5 h [sample c (1.52 mol-% Ag)], 8 h [sample d (4.60 mol-% Ag)], and 10 h [sample e (5.54 mol-% Ag)].

ples d (4.60 mol-% Ag) and e (5.54 mol-% Ag)] begins to decrease, but is still higher than that of the uncoated Fe_3O_4-@TiO_2 microspheres (sample a). Figure 7 (b) shows the first-order degradation rates of methylene blue (MB) and the reaction rate constants (inset). From these data, we can obtain the reaction rate constants of the samples a, b, c, d, and e for MB degradation, which are 0.037, 0.077, 0.134, 0.083, and 0.063 min^{-1}, respectively. These results indicate that sample c achieved the delicate balance between the enhancement of charge-separation and the decrease in the active surface area. Thus, sample c was used as a reference for comparison of the photocatalytic activity for MB degradation with other samples in the following experiments.

2.2.2 Comparison of Photocatalytic Activity Between Different Photocatalysts

Commercial TiO_2 (Degussa P25 titania), which is known to be the best photocatalyst commercially available, was used as a reference to qualitatively understand the photocatalytic activities of the as-prepared samples.

Figure 8 (a) shows the changes in the absorption spectra of an aqueous MB solution (1.0×10^{-5} M) exposed to UV light for various times in the presence of Ag-coated Fe_3O_4@TiO_2 microspheres. Under UV illumination, a rapid decrease of MB absorption at 665 nm was observed. The MB degradation rate was very fast at the beginning of the irradiation and became slow. A sharp decrease of the major absorption band within 30 min indicates that this sample exhibits excellent photocatalytic activity for the degradation of MB.

Figure 8 (b) displays the photocatalytic degradation of MB as a function of time on different catalysts. A sample in the absence of catalyst is also included. In addition, the Fe_3O_4 microspheres were also immersed in MB aqueous solution (1.0×10^{-5} M) for 0.5 h to ensure that the products reached adsorption equilibrium, then photodegradation of MB under UV irradiation was performed in order to evaluate its photocatalytic activity (Figure S4). In Figure S4, we can see that adsorption and photodegradation of MB with the Fe_3O_4 microspheres is negligible. As shown in Figure 8 (b), the photocatalytic activity of Ag-coated Fe_3O_4@TiO_2 microspheres is much higher than that of Degussa P25 titania and the Fe_3O_4@TiO_2 microspheres. The deposition of metallic Ag nanoparticles on the surface of the Fe_3O_4@TiO_2 microspheres increases the photocatalytic activity, which indicates that the Ag–TiO_2 heterojunction can improve electron-charge separation efficiency.[35] In order to study annealing effects on the photocatalytic performance of the catalysts, the Fe_3O_4@TiO_2 (anatase) microspheres and Ag-coated Fe_3O_4@TiO_2 (anatase) microspheres were both annealed at 450 °C for 3 h in an argon shield atmosphere. It can be seen from Figure S5 that both the annealed samples are photoactive; however, both have lower photocatalytic activity than that of the unannealed catalysts, which suggests that annealing deteriorates the photocatalytic activity. This can be attributed to the heat treatment of iron oxide/titania (anatase) systems that can give rise to unfavorable heterojunction interactions between the magnetic core and the titania (anatase) coating, which leads to an increase in electron-hole recombination and photodissolution.[14–18] This would negatively affect the activity of the catalyst. Another important disadvantage of the annealed composite is that its surface properties are worse. During the heat treatment of the composites, there is a loss of the surface hydroxy groups on TiO_2, which reduces the

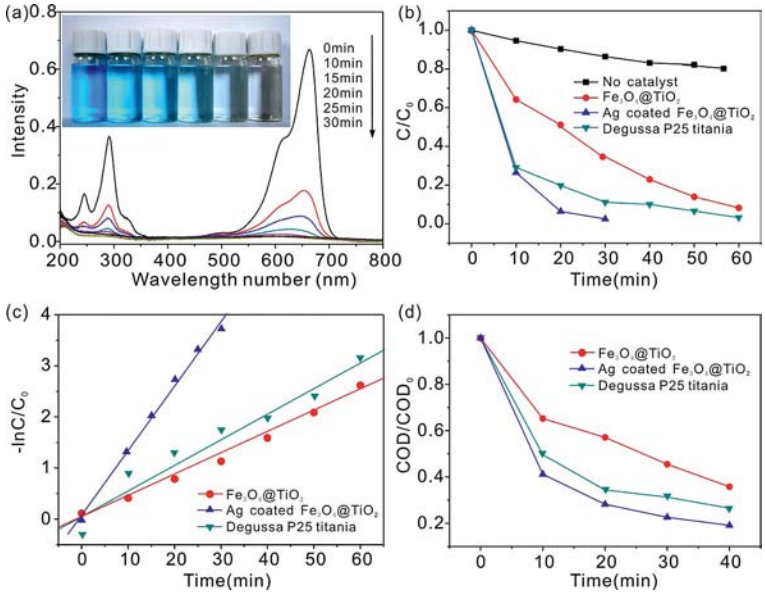

Figure 8. (a) Time-dependent optical absorbance spectra and photograph (inset) of the MB solution (starting concentration: 1.0×10^{-5} M) in the presence of Ag-coated Fe_3O_4@TiO_2 microspheres after exposure to UV light for different durations. (b) The kinetic curve of photodegradation of MB solution for different samples. (c) Comparison of first-order degradation rates for MB degradation for different samples. (d) Time-dependent changes in COD/COD_0 for different samples.

number of active sites for the photocatalytic reaction.[20,36–37] The weak photoactivities in the annealed microspheres can partially be attributed to the loss of the surface hydroxy groups on TiO_2. This is consistent with the results of X-ray photoelectron spectroscopy (not shown). These results suggest that directly immobilizing anatase TiO_2 nanoparticles on to the surface of magnetic microspheres is beneficial in retaining the excellent activity of the catalyst.

The kinetics of these photocatalytic reactions can be described as pseudo first order:

$$-\ln\frac{C}{C_0} = kt$$

where C_o and C are MB concentrations initially and after time t, respectively (Figure 8 c), and the rate constants (k, min^{-1}) were determined from plots of $\ln(C/C_o)$ vs. irradiation time. Of the photocatalysts tested, the Ag-coated Fe_3O_4@TiO_2 microspheres have the largest rate constants.

In order to investigate the efficiencies of mineralization for MB in these three catalysts, the chemical oxygen demand (COD) was also measured during the reaction. Figure 8 (d) shows the COD-removal efficiencies of dye waste water after 40 min. From these results, it is worth noting that the Ag-coated Fe_3O_4@TiO_2 microspheres are the strongest at mineralizing MB among the catalysts. The results also illustrate that COD-removal efficiency had the same trend as the removal efficiency of color in three different catalysts. However, the color-removal efficiencies are much higher than the corresponding COD-removal efficiencies. The maximum COD-removal efficiency for the Ag-coated Fe_3O_4@TiO_2 microspheres is about 81%, whereas the color completely disappears after 40 min. The high color-removal efficiency and low COD-removal efficiency illustrates that only chromophores are destroyed and reduced instead of completely mineralizing organic pollutants to CO_2 and H_2O. On the other hand, the results also indirectly illustrate the degradation of intermediate products in the process.

2.2.3 Photocatalyst Reuse

As practical recyclable catalysts, high catalytic activity in each cycle is necessary. Renewable photocatalytic activity was also investigated, and the results are presented in Figure 9. We can see that the kinetic rate constant of the Ag-coated Fe_3O_4@TiO_2 microspheres is very stable. After the degradation experiment was carried out five times, the cyclic degradation reaction rate constant was still higher than 0.1 min^{-1}. Thus, the as-prepared catalyst can be used as a photocatalyst in practical applications.

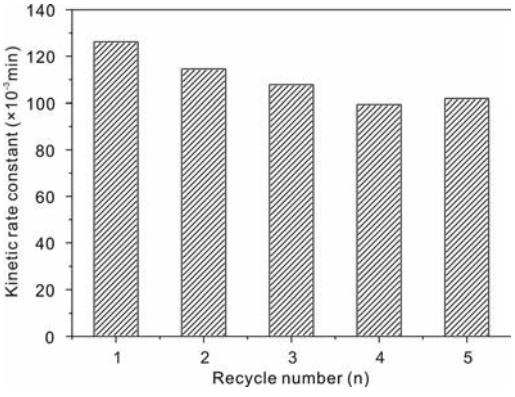

Figure 9. Cyclic degradation reaction rate constants for MB degradation of Ag-coated Fe_3O_4@TiO_2 microspheres.

3. Conclusions

We have reported a simple, green, efficient method for the preparation of uniform Ag-coated Fe_3O_4@TiO_2 microspheres. The sample has a high BET surface area, a large number of pore channels, and excellent magnetic properties at room temperature. Ag nanoparticle loading can be controlled by the UV photoreduction time; the photocatalytic activity reached a maximum when the exposure time was 5 h. It was demonstrated that the rate of photodegradation of MB is superior to that of Degussa P25 titania and uncoated Fe_3O_4@TiO_2 microspheres, which is attributed to the Ag–TiO_2 heterojunction of the Ag-coated Fe_3O_4@TiO_2 microspheres. After recycling the photocatalyst five times for MB photodegradation, the degradation reaction rate constant of the Ag-coated Fe_3O_4@TiO_2 microspheres was stable. This means that the as-prepared composites can be used as convenient, recyclable photocatalysts.

Experimental Section

All reagents were commercially available from Sinopharm Chemical Reagent Co., Ltd (China). The reagents were of analytical grade and used without further purification. Degussa P25 titania was purchased from Guangzhou Huali Sen Trading Co., Ltd.

Preparation of Fe_3O_4 Microspheres: The synthesis was carried out according to a previous report with a little modification.[38] In a typical procedure, $FeCl_3{\cdot}6H_2O$ (1.35 g) was dissolved in ethylene glycol (40 mL) to form a clear solution. Polyethylene glycol 10000 (1.0 g) and $NaAc{\cdot}3H_2O$ (3.6 g) were added. The mixture was stirred until the reactants were fully dissolved before the mixture was transferred into a Teflon®-lined autoclave with a capacity of 50 mL and heated at 200 °C for 10 h. The products were separated with magnet, rinsed with deionized water and ethanol, and dried under vacuum at 50 °C for 6 h.

Preparation of Fe_3O_4@TiO_2 Core/Shell Microspheres: The Fe_3O_4@TiO_2 core/shell microspheres were prepared by the vapor–thermal method using TBOT as the titanium source.[29,39–40] In a typical procedure, as-prepared Fe_3O_4 microspheres (25 mg) were dispersed in ethanol and TBOT before being transferred into a 10 mL beaker, which was placed into a 60 mL stainless steel autoclave with a Teflon® liner. The free space between the Teflon® liner and the beaker was filled with distilled water. After sealing, the autoclave was heated to 150 °C for 10 h. During the reaction, the distilled water vaporized and hydrolyzed the TBOT. At the end of the reaction, the autoclave was cooled to room temperature, and the precipitate obtained was repeatedly washed with distilled water and ethanol and dried at 50 °C in a vacuum oven for 6 h.

Preparation of Ag-Coated Fe_3O_4@TiO_2 Core/Shell Microspheres: Fe_3O_4@TiO_2 core/shell microspheres (50 mg) were dispersed in a

0.2 M $Ag(NH_3)_2^+$ solution (60 mL), and the solution was stirred mechanically for 0.5 h to ensure sufficient adsorption of $Ag(NH_3)_2^+$ by the microspheres. The solution was exposed to UV radiation from a 250 W high-pressure Hg lamp (main wavelength: 365 nm) at room temperature for several hours. The final products were separated magnetically, washed, and dried under vacuum at 50 °C for 6 h.

Photocatalytic Activity Measurement of Ag-Coated Fe_3O_4@TiO_2 Core/Shell Microspheres: MB is a dye, which exhibits toxic effects on microbial populations and can be toxic and carcinogenic to mammals. It was chosen as a model pollutant to evaluate the photocatalytic activity of the as-prepared catalysts. In the photocatalytic experiments, Ag-coated Fe_3O_4@TiO_2 core/shell microspheres (10 mg) were added to an aqueous MB solution (10 mL, 1×10^{-5} M), and the reaction mixture was stirred in the dark for 0.5 h to ensure the adsorption/desorption equilibrium of the dye with the microspheres. Subsequently, the solution was exposed to UV radiation from a 15 W low-pressure Hg lamp with the main emission wavelength at 254 nm at room temperature. The samples exposed to the UV light for different time intervals were removed from the reaction suspension, separated magnetically, and analyzed with a UV/Vis spectrophotometer to investigate the photodegradation of MB. The progress in photodegradation (P_1) with irradiation time was calculated using the following equation:

$$P_1 = \frac{C}{C_0} = \frac{A}{A_0}$$

where C_0 represents the initial concentration, C the changed concentration, A_0 the initial absorbance, and A the changed absorbance of MB at the characteristic absorption wavelength of 665 nm.

The progress in photodegradation (P_2) with irradiation time can be calculated as follows:

$$P_2 = \frac{\mathrm{COD}}{\mathrm{COD}_0}$$

where COD represents the COD value in the solution after reaction and COD_0 is the COD in the initial solution. To evaluate the photoactivity of the Ag-coated Fe_3O_4@TiO_2 core/shell microsphere, equal amounts of Degussa P25 titania and uncoated Fe_3O_4@TiO_2 core/shell microspheres were used to catalyze the solution of MB under the same conditions.

Characterization: Field emission scanning electron microscope (FESEM) images were taken with a FESEM (Quanta 200 FEG) operated at an accelerating voltage of 10.0 kV. HRTEM images were obtained with a JEM-2010 HRTEM equipped with an X-ray EDS working at an acceleration voltage of 200 kV. In order to prove the presence of both TiO_2 and Ag nanoparticles on the surface of Fe_3O_4 microsphere, samples were analyzed by elemental mapping image analysis on the same TEM. In this analysis, when the electron beam is incident into a specimen, part of the beam is inelastically scattered and loses a fraction of the energy. The distribution of elements in a specimen is clarified by selecting and imaging the electrons with a specific energy loss. X-ray scattering patterns were scanned by analyzing powder samples with a Philips X'Pert Pro X-ray diffractometer with Cu-K_α radiation (1.5418 Å). The specific surface areas of the as-prepared products were measured with a Micromeritics ASAP 2020 M$^+$C BET equipment using nitrogen adsorption and desorption. The magnetic properties of the samples were investigated using a vibrating sample magnetometer with an applied field between –5000 and 5000 Oe at room temperature (BHV-55, Riken, Japan). UV/Vis spectra were recorded with a Shimadzu UV-2550 spectrophotometer. COD was analyzed with a COD Analyzer Model HH-5 (Jiangsu, China).

Supporting Information (see footnote on the first page of this article): The effect of water vapor on the hydrolysis of TBOT at different temperatures, the effect of the amount of TBOT in the reaction medium on the thickness of the TiO_2 shell, the effect of a $AgNO_3$ reaction medium on the Ag nanoparticle dispersion, photodegradation of MB with Fe_3O_4 microspheres, the effect of annealing on the photocatalytic activity.

Acknowledgments

This work was supported by the One Hundred Person Project of the Chinese Academy of Sciences, China and the National Key Scientific Program – Nanoscience and Nanotechnology (grant number 2011CB933700).

[1] A. Heller, *Acc. Chem. Res.* **1995**, *28*, 503–508.
[2] M. R. Hoffmann, S. T. Martin, W. Y. Choi, D. W. Bahnemann, *Chem. Rev.* **1995**, *95*, 69–96.
[3] A. L. Linsebigler, G. Q. Lu, J. T. Yates, *Chem. Rev.* **1995**, *95*, 735–758.
[4] H. X. Li, Z. F. Bian, J. Zhu, D. Q. Zhang, G. S. Li, Y. N. Huo, H. Li, Y. F. Lu, *J. Am. Chem. Soc.* **2007**, *129*, 8406–8407.
[5] D. H. Chen, L. Cao, F. Z. Huang, P. Imperia, Y. B. Cheng, R. A. Caruso, *J. Am. Chem. Soc.* **2010**, *132*, 4438–4444.
[6] L. Li, C. Y. Liu, *J. Phys. Chem. C* **2010**, *114*, 1444–1450.
[7] J. G. Yu, Y. R. Su, B. Cheng, *Adv. Funct. Mater.* **2007**, *17*, 1984–1990.
[8] H. Y. Yang, S. F. Yu, S. P. Lau, X. W. Zhang, D. D. Sun, G. Jun, *Small* **2009**, *5*, 2260–2264.
[9] H. M. Zhu, B. F. Yang, J. Xu, Z. P. Fu, M. W. Wen, T. Guo, S. Q. Fu, J. Zuo, S. Y. Zhang, *Appl. Catal. B* **2009**, *90*, 463–469.
[10] L. X. Yang, S. L. Luo, Y. Li, Y. Xiao, Q. Kang, Q. Y. Cai, *Environ. Sci. Technol.* **2010**, *44*, 7641–7646.
[11] H. F. Zhuang, C. J. Lin, Y. K. Lai, L. Sun, J. Li, *Environ. Sci. Technol.* **2007**, *41*, 4735–4740.
[12] M. Srinivasan, T. White, *Environ. Sci. Technol.* **2007**, *41*, 4405–4409.
[13] C. X. Wang, L. W. Yin, L. Y. Zhang, L. Kang, X. F. Wang, R. Gao, *J. Phys. Chem. C* **2009**, *113*, 4008–4011.
[14] Y. Gao, B. H. Chen, H. L. Li, Y. X. Ma, *Mater. Chem. Phys.* **2003**, *80*, 348–355.
[15] D. Beydoun, R. Amal, G. Low, S. McEvoy, *J. Mol. Catal. A* **2002**, *180*, 193–200.
[16] D. Beydoun, R. Amal, *Mater. Sci. Eng. B* **2002**, *94*, 71–81.
[17] P. M. Alvarez, J. Jaramillo, F. Lopez-Pinero, P. K. Plucinski, *Appl. Catal. B* **2010**, *100*, 338–345.
[18] S. H. Xu, W. F. Shangguan, J. Yuan, M. X. Chen, J. W. Shi, *Appl. Catal. B* **2007**, *71*, 177–184.
[19] S. Watson, D. Beydoun, R. Amal, *J. Photochem. Photobiol. A: Chem.* **2002**, *148*, 303–313.
[20] S. W. Lee, J. Drwiega, C. Y. Wu, D. Mazyck, W. M. Sigmund, *Chem. Mater.* **2004**, *16*, 1160–1164.
[21] S. H. Xuan, W. Q. Jiang, X. L. Gong, Y. Hu, Z. Y. Chen, *J. Phys. Chem. C* **2009**, *113*, 553–558.
[22] Y. P. He, Z. Y. Zhang, Y. P. Zhao, *J. Vac. Sci. Technol. B* **2008**, *26*, 1350–1358.
[23] J. Sa, M. Fernandez-Garcia, J. A. Anderson, *Catal. Commun.* **2008**, *9*, 1991–1995.
[24] H. Tada, T. Mitsui, T. Kiyonaga, T. Akita, K. Tanaka, *Nat. Mater.* **2006**, *5*, 782–786.
[25] E. Formo, E. Lee, D. Campbell, Y. N. Xia, *Nano Lett.* **2008**, *8*, 668–672.
[26] T. Hirakawa, P. V. Kamat, *J. Am. Chem. Soc.* **2005**, *127*, 3928–3934.

[27] Y. Tian, T. Tatsuma, *J. Am. Chem. Soc.* **2005**, *127*, 7632–7637.
[28] J. M. Du, J. L. Zhang, Z. M. Liu, B. X. Han, T. Jiang, Y. Huang, *Langmuir* **2006**, *22*, 1307–1312.
[29] Y. R. Su, J. G. Yu, J. Lin, *J. Solid State Chem.* **2007**, *180*, 2080–2087.
[30] B. B. Huang, Z. K. Zheng, X. Y. Qin, X. Y. Zhang, Y. Dai, M. H. Whangbo, *J. Mater. Chem.* **2011**, *21*, 9079–9087.
[31] B. B. Huang, Z. K. Zheng, X. Y. Qin, X. Y. Zhang, Y. Dai, *Chem. Eur. J.* **2010**, *16*, 11266–11270.
[32] A. Kudo, Y. Miseki, *Chem. Soc. Rev.* **2009**, *38*, 253–278.
[33] K. S. W. Sing, R. A. W. Haul, L. Moscou, R. A. Pierotti, J. Rouquerol, T. Siemieniewska, *Pure Appl. Chem.* **1985**, *57*, 603–619.
[34] T. Hirakawa, P. V. Kamat, *J. Am. Chem. Soc.* **2005**, *127*, 3928–3934.
[35] W. Smith, S. Mao, G. H. Lu, A. Catlett, J. H. Chen, Y. P. Zhao, *Chem. Phys. Lett.* **2010**, *485*, 171–175.
[36] E. Sanchez, T. Lopez, R. Gomez, Bokhimi, A. Morales, O. Novaro, *J. Solid State Chem.* **1996**, *122*, 309–314.
[37] V. M. Gunko, V. I. Zarko, E. Chibowski, V. V. Dudnik, R. Leboda, V. A. Zaets, *J. Colloid Interface Sci.* **1997**, *188*, 39–57.
[38] H. Deng, X. L. Li, Q. Peng, X. Wang, J. P. Chen, Y. D. Li, *Angew. Chem.* **2005**, *117*, 2842; *Angew. Chem. Int. Ed.* **2005**, *44*, 2782–2785.
[39] X. X. Yu, J. G. Yu, B. Cheng, M. Jaroniec, *J. Phys. Chem. C* **2009**, *113*, 17527–17535.
[40] Q. Zhang, W. Fan, L. Gao, *Appl. Catal. B* **2007**, *76*, 168–173.

Received: July 9, 2011
Published Online: October 11, 2011

